Available online at www.CivileJournal.org

Civil Engineering Journal

(E-ISSN: 2476-3055; ISSN: 2676-6957)

Vol. 12, No. 05, May, 2026

Comparative Assessment of Soil Salinity Using Sentinel-2 and Landsat-7 Remote Sensing Data

Mohamed A. Elshewy [1], Mohamed Freeshah [2, 3*], Mostafa H. A. Mohamed [1], Mahmoud M. E. Gad [4], Mervat M. Refaat [3, 4]

[1] *Department of Civil Engineering, Faculty of Engineering, Al-Azhar University, Cairo 11751, Egypt.*

[2] *Civil and Environmental Engineering Department, College of Engineering, UAE University, Al Ain 15551, United Arab Emirates.*

[3] *Geomatics Engineering Department, Faculty of Engineering at Shoubra, Benha University, Cairo 11629, Egypt.*

[4] *Civil Engineering Department, Canadian International College, Cairo, Egypt.*

Received 03 January 2026; Revised 19 April 2026; Accepted 23 April 2026; Published 01 May 2026

Abstract

This study evaluates the performance of the Sentinel-2 multi-spectral instrument (MSI) and Landsat-7 Enhanced Thematic Mapper Plus (ETM+) for soil salinity mapping across contrasting agroecosystems in Egypt, with particular emphasis on subsurface salinity conditions (>0.5 m). A multi-stage calibration framework was implemented, in which historical Landsat-5 imagery (1995) was first integrated with field-measured electrical conductivity (EC) data to establish a spectral baseline. This baseline was subsequently applied to Sentinel-2 and Landsat-7 imagery acquired in 2015 and validated using in-situ total dissolved solids (TDS) measurements. Among the evaluated spectral indices, Salinity Index 5 (SI5) demonstrated the strongest relationship with field data and was selected for salinity mapping. Comparative analysis revealed that Sentinel-2 significantly outperforms Landsat-7, achieving a higher predictive accuracy ($R^2 = 0.89$) compared to Landsat-7 ($R^2 = 0.72$), primarily due to its finer spatial resolution (10 m) and reduced mixed-pixel effects. In addition, the application of second-degree polynomial regression substantially improved model performance relative to linear approaches, confirming the non-linear nature of soil salinity–spectral relationships. The results further indicate that surface spectral indices can provide meaningful estimates of subsurface salinity under specific environmental conditions. Overall, the integration of multi-temporal satellite data, robust spectral indices, and non-linear modeling provides an effective framework for soil salinity assessment in arid environments. This approach enhances the reliability of remote sensing-based monitoring and supports sustainable land management in salinity-affected regions.

Keywords: Soil Salinity; Electrical Conductivity; Soil Salinity Indices; Total Dissolved Salts; Sentinel-2; Landsat-7; GIS and Remote Sensing.

1. Introduction

Soil constitutes a finite and non-renewable resource essential for sustaining terrestrial ecosystems and agricultural productivity [1–3]. However, soil degradation, particularly salinization, poses a significant threat to sustainable land use, especially in arid and semi-arid regions [4–6]. Soil salinity, defined as the accumulation of soluble salts in the soil profile, adversely affects plant growth, reduces crop yields, and can ultimately render land unproductive [7]. This process is largely irreversible on human timescales, making its monitoring and management a critical component of sustainable development strategies [8, 9]. In Egypt, soil salinization represents a pervasive

* Corresponding author: mfreeshah@uaeu.ac.ae

https://doi.org/10.28991/CEJ-2026-012-05-021

and escalating environmental challenge [10]. The country's agricultural systems are largely concentrated in the Nile Delta and desert oases, where irrigation-dependent farming dominates. It is estimated that approximately 30–50% of Egypt's cultivated land is affected by varying degrees of salinity [11]. Furthermore, climate change-induced sea-level rise has intensified seawater intrusion into the Nile Delta, posing an additional threat to soil quality and long-term agricultural sustainability [12].

Traditional methods for assessing soil salinity rely primarily on field sampling and laboratory-based measurements, such as electrical conductivity (EC) analysis [13]. While these approaches provide accurate point-based observations, they are labor-intensive, time-consuming, and often impractical for large-scale or continuous monitoring. Consequently, there is a growing need for efficient, scalable, and cost-effective techniques capable of capturing the spatial and temporal variability of soil salinity across extensive regions.

Remote sensing (RS) provides a synoptic and repeatable framework for detecting salinity through spectral responses of soils and vegetation. RS enables the indirect detection of salinity through variations in reflectance characteristics and vegetation stress indicators [14, 15]. Over the past two decades, multispectral satellite systems, including Landsat and Sentinel missions, have been extensively utilized for soil salinity assessment at regional and global scales. These sensors provide valuable data across visible, near-infrared (NIR), and shortwave infrared (SWIR) wavelengths, which are particularly sensitive to salt minerals and salinity-induced changes in soil and vegetation properties. Recent advances in remote sensing have demonstrated the increasing importance of integrating multi-source observational systems for environmental monitoring. For example, spaceborne global navigation satellite systems (GNSS)-based remote sensing techniques have shown strong potential for detecting complex geophysical phenomena through signal-based analysis, highlighting the value of combining different sensing modalities to improve spatial and temporal coverage [16–18]. Similarly, the use of real GNSS data for detecting atmospheric and ionospheric disturbances further emphasizes the capability of remote sensing technologies to capture subtle environmental variations through indirect signal responses [19–22].

On the other side, numerous studies have demonstrated the effectiveness of spectral band combinations and indices in detecting saline soils and salt-affected vegetation [23]. For instance, visible and infrared band ratios have been widely used to enhance salinity signals, while specific Landsat bands (e.g., thematic mapper (TM) bands 3, 4, 5, and 7) have been identified as particularly informative for salt mineral detection [24–26]. Additionally, the integration of thermal bands has been shown to improve discrimination in cases of spectral ambiguity [27]. In the Egyptian context, remote sensing studies have successfully mapped salinity patterns in regions such as the Nile Delta and Siwa Oasis, revealing characteristic spectral signatures associated with salt-affected soils [12, 28]. However, many of these early efforts were constrained by moderate spatial resolution (30 m) and the reliance on relatively simple statistical models [29–31].

Recent advancements in satellite technology, particularly the launch of Sentinel-2 with its multi-spectral instrument (MSI), have significantly enhanced the potential for soil salinity monitoring [32]. Sentinel-2 offers higher spatial resolution (10–20 m) and improved spectral capabilities compared to earlier Landsat sensors, enabling more detailed characterization of heterogeneous landscapes [22, 33]. Despite these improvements, several challenges remain in the application of remote sensing for soil salinity assessment [34].

First, there is a notable lack of rigorous comparative studies between legacy systems such as Landsat-7 and newer platforms like Sentinel-2. While Landsat-8 has been widely evaluated, Landsat-7 remains critical for long-term environmental monitoring due to its historical continuity [35–37]. Second, most existing research focuses predominantly on surface salinity (typically within the top 5–15 cm), where salt crusts are readily detectable [38–40]. In contrast, subsurface salinity, often occurring at depths of 0.5–1.5 m and directly affecting root-zone processes, remains insufficiently investigated, particularly in irrigated agricultural systems [41]. Third, the majority of studies rely on simple linear regression (SLR) models to relate spectral indices to salinity indicators such as EC or total dissolved solids (TDS). Although computationally efficient, these models often fail to capture the inherent non-linear relationships governing soil–water–salt interactions, especially in complex soil environments such as calcareous and clay-rich soils prevalent in Egypt [42].

In response to these limitations, this study presents a comprehensive comparative assessment of soil salinity derived from Sentinel-2 and Landsat-7 data in two representative regions of Egypt [43–45]. The proposed methodology integrates a multi-temporal and multi-sensor framework designed to enhance the accuracy and robustness of salinity estimation. Specifically, the study employs (i) a historical baseline calibration using Landsat-5 imagery and legacy field data to identify optimal spectral salinity indices, (ii) cross-sensor validation using Sentinel-2 and Landsat-7 datasets to evaluate the impact of spatial resolution on retrieval performance, and (iii) advanced modeling approaches, including polynomial and exponential functions, to better capture non-linear relationships and improve the estimation of

subsurface salinity conditions [46]. By addressing both methodological and data-related gaps, this research contributes to the advancement of digital soil mapping and supports the development of more effective monitoring strategies for salinity-affected regions in arid environments.

2. Study Area and Datasets

2.1. Study Areas

The selection of multiple study areas is essential for evaluating the spatial variability and controlling factors of soil salinization under different environmental conditions. By analyzing regions with contrasting geomorphological, soil, and hydrological characteristics, this study aims to provide a more comprehensive understanding of salinity dynamics and their implications for agricultural sustainability.

The first study area is located within Al-Beheira Governorate in the western Nile Delta, Egypt (Figure 1), and is geographically bounded by longitudes 29°44′30″–29°51′30″ E and latitudes 31°05′00″–31°10′00″ N. This area was selected based on data availability from the Japan International Cooperation Agency (JICA) project on the El-Omoum main drainage improvement conducted in the mid-1990s, for more information we can refer to https://openjicareport.jica.go.jp/pdf/11260965_01.pdf (accessed on April 2026). The region is characterized by a flat alluvial plain dominated by heavy clay soils, which are prone to waterlogging and secondary salinization due to poor drainage conditions, shallow groundwater levels, and high evaporation rates. These characteristics make the area representative of typical salinity-affected agricultural lands in the Nile Delta [47].

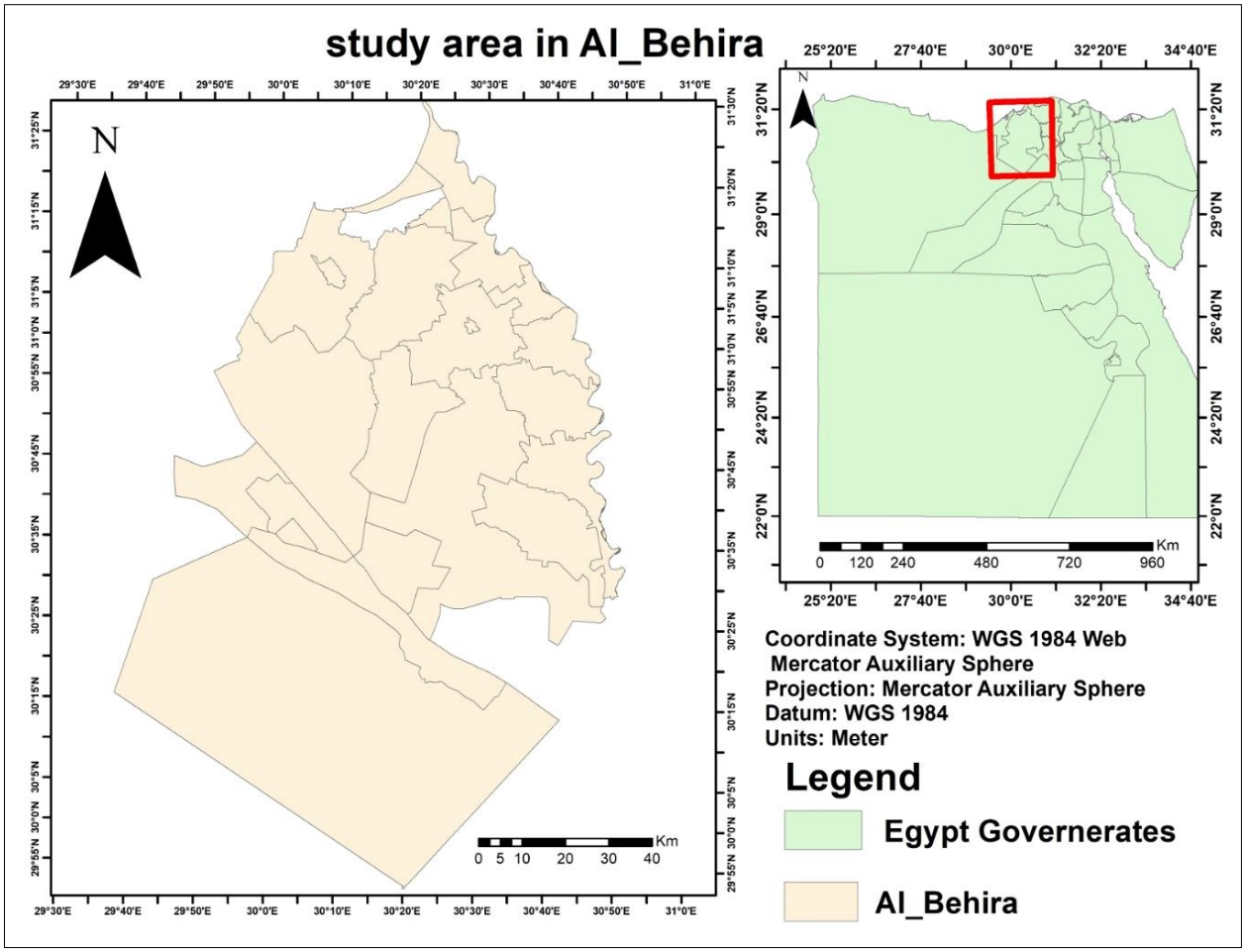

Figure 1. Location of the first study area in Al-Beheira Governorate, Egypt

The second study area is located in northeastern Egypt, Al-Dakahlia Governorate extending east of the Nile Delta toward the Sinai Peninsula (Figure 2), between longitudes 31°30′–33°10′ E and latitudes 30°20′–31°30′ N. This region encompasses the El-Tina Plain and adjacent desert landscapes, where geomorphological conditions vary from flat coastal plains to inland aeolian sand formations. Unlike the first study area, soils in this region are predominantly sandy to sandy-loam, with lower water retention capacity but higher susceptibility to salinity

accumulation due to shallow saline groundwater and residual marine deposits (sabkha conditions). Groundwater salinity in the second study area is typically elevated due to marine intrusion and shallow saline aquifers, contributing significantly to soil salinization processes. Agricultural development in this area relies primarily on the El-Salam Canal, which conveys a mixture of Nile freshwater and agricultural drainage water, necessitating careful salinity management.

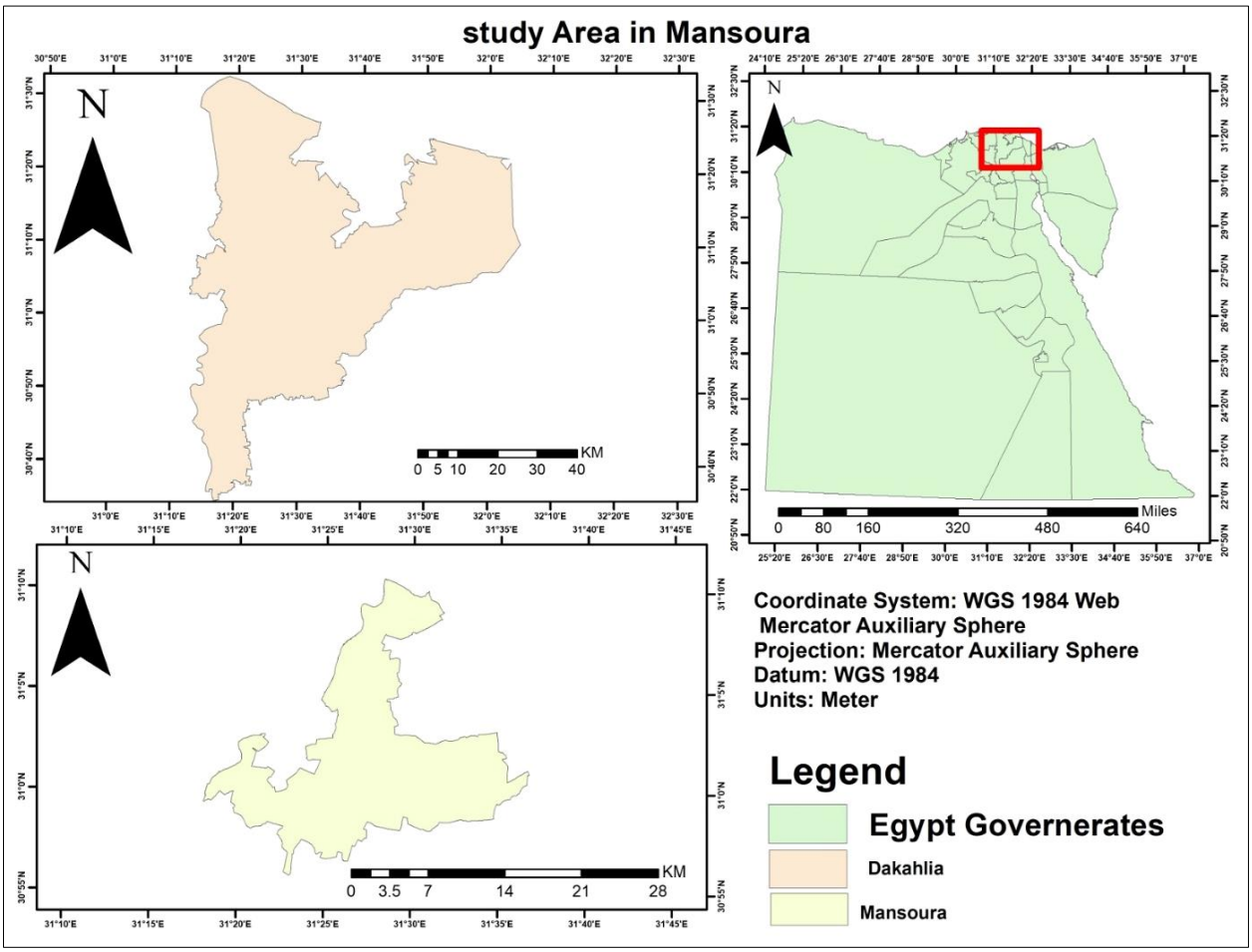

Figure 2. Location of the second study area in Al-Dakahlia Governorate, northeastern Egypt

The climate of both study areas is arid to semi-arid, characterized by high temperatures, low precipitation, and high evapotranspiration rates. During the field survey conducted in August 2015, the average air temperature was approximately 31°C, with relative humidity around 61%, and no recorded rainfall. These climatic conditions contribute significantly to salt accumulation in the soil profile, particularly under irrigation practices.

The comparative analysis of these two contrasting environments, clay-rich alluvial soils in the Nile Delta and sandy coastal/desert soils in northeastern Egypt, provides a robust framework for evaluating the performance of remote sensing techniques in detecting and modeling soil salinity across different land-use and soil conditions.

2.2. Field Data

Ground truth data for the first study area were obtained from field surveys conducted in September 1995 by the Japan International Cooperation Agency (JICA) in the West Nile Delta as part of the El-Omoum main drainage improvement project. Soil samples were collected at depths not exceeding 0.5 m, and their electrical conductivity (EC) was measured under laboratory conditions. The spatial distribution of the sampling locations is presented in Figure 3 [47].

For the second study area, field investigations were carried out in August 2015 by Mohram-Bakhom Consultant Office during the Mansoura–Damietta railway development project. A total of nine soil samples were collected at depths of approximately 1 m using auger drilling. The sampling locations were distributed along the railway alignment connecting Mansoura and Damietta, as shown in Figure 4.

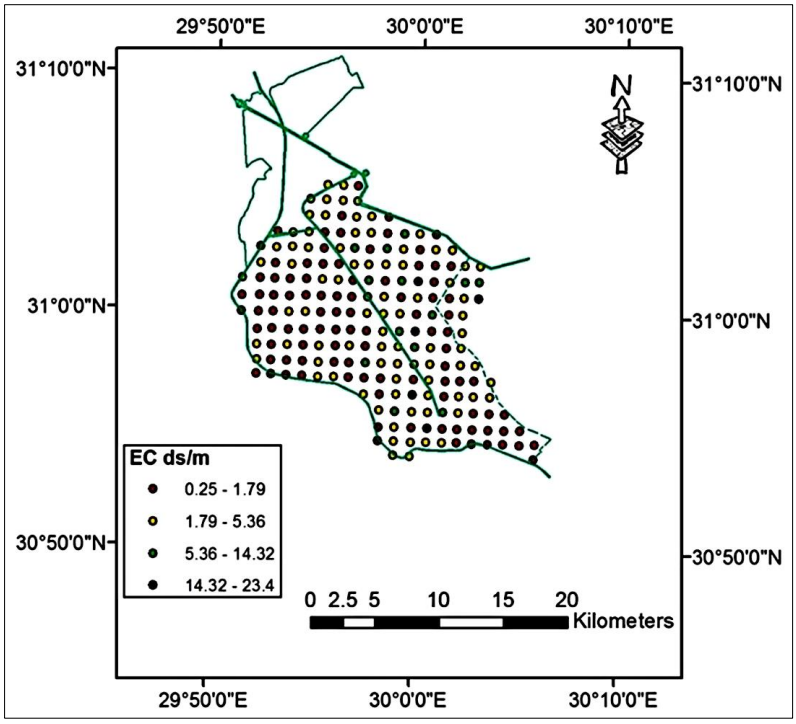

Figure 3. Locations of soil sampling points for the first study area, projected in WGS 84 / UTM Zone 36N

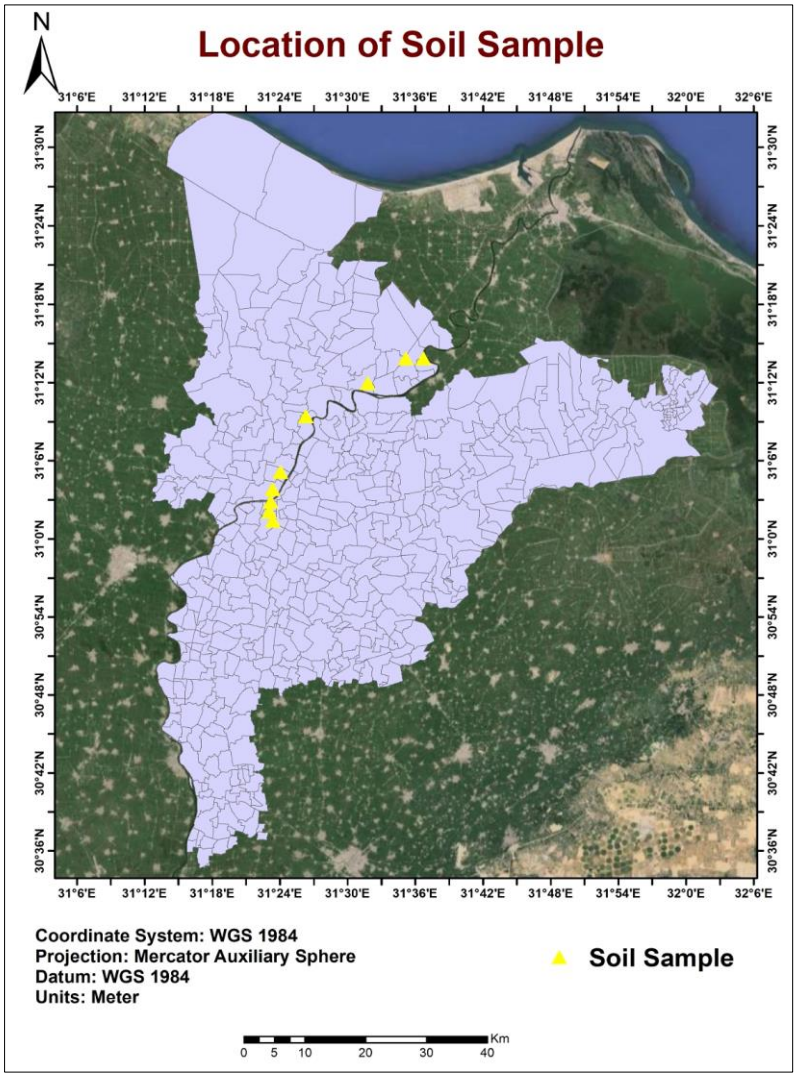

Figure 4. Locations of soil sampling points for the second study area

The collected samples were analyzed in the laboratory to determine total dissolved solids (TDS), which ranged from 1260 to 14,800 mg/L, indicating significant spatial variability in soil salinity. The spatial distribution of these sampling points is illustrated in Figure 4.

2.3. Satellite Datasets

This study integrates multi-source remote sensing data with ground-based measurements to assess soil salinity across two contrasting regions in Egypt. The combined use of satellite imagery and field observations enables a robust evaluation of spatial variability and enhances the reliability of salinity estimation models.

Three satellite datasets were utilized: (1) Landsat 5 TM, acquired on 26 September 1995, with a spatial resolution of 30 m, (2) Sentinel-2 MSI, acquired on 13 August 2015, with a spatial resolution of 10 m, and (3) Landsat 7 Enhanced Thematic Mapper Plus (ETM+), acquired on 24 August 2015, with a spatial resolution of 30 m. The acquisition dates were selected to closely correspond with the timing of field data collection, ensuring consistency between satellite observations and ground measurements.

All satellite images were geometrically corrected and projected to the World Geodetic System 1984 (WGS 84) using the Universal Transverse Mercator (UTM) Zone 36N coordinate system. Landsat data were obtained from the United States Geological Survey (USGS) archive, while Sentinel-2 imagery was selected with cloud coverage less than 10% to minimize atmospheric interference (see Figure 5).

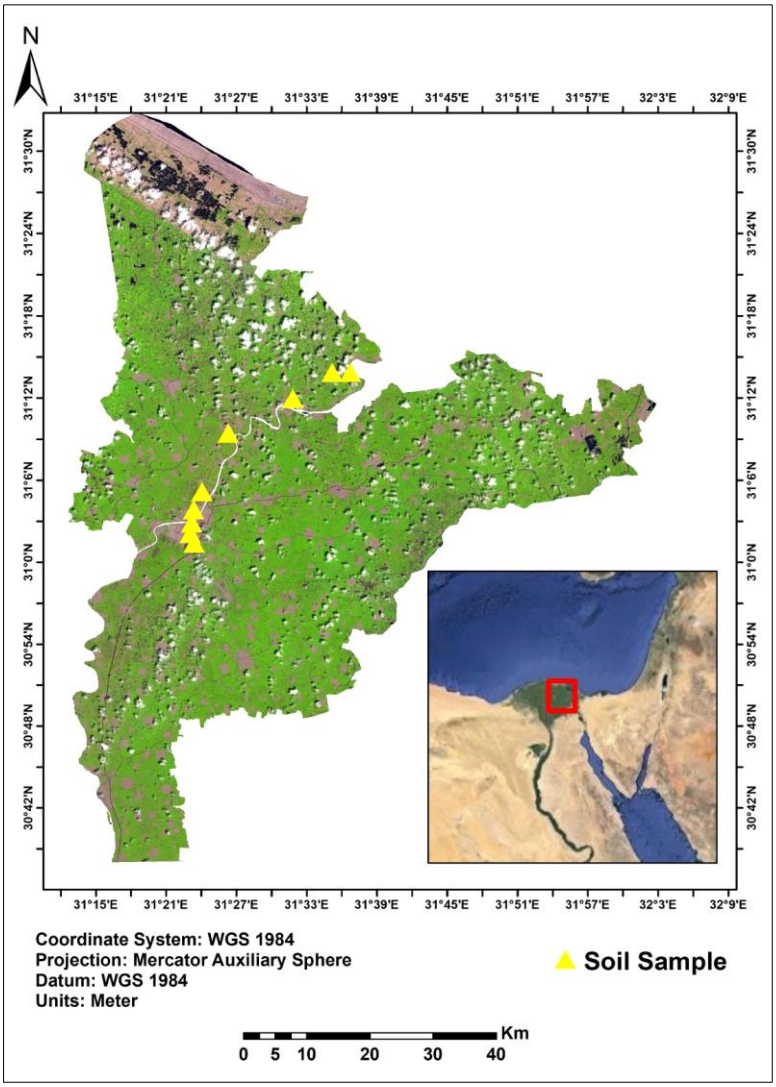

Figure 5. Overview of remote sensing datasets used in this study, including Sentinel-2, Landsat 7, and Landsat 5 imagery

The Landsat 7 ETM+ image, with cloud coverage below 10%, is presented in Figure 6, where soil sampling locations are indicated.

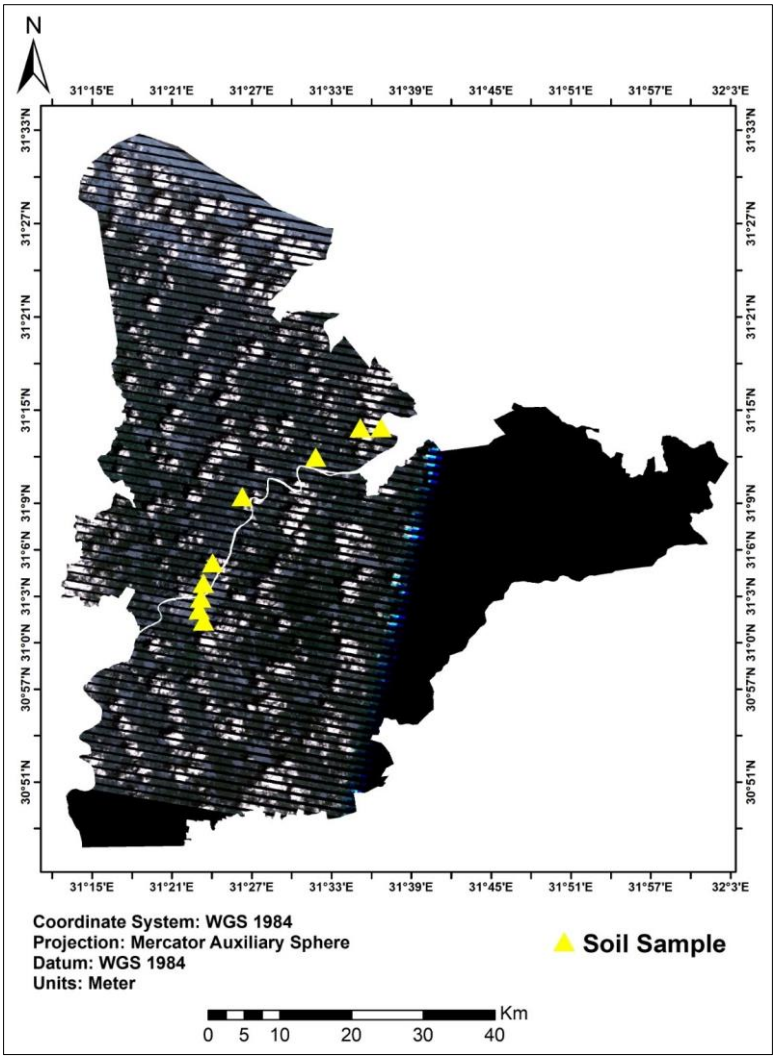

Figure 6. Landsat 7 ETM+ image showing soil sampling locations

Similarly, the Landsat 5 TM image for the first study area is shown in Figure 7.

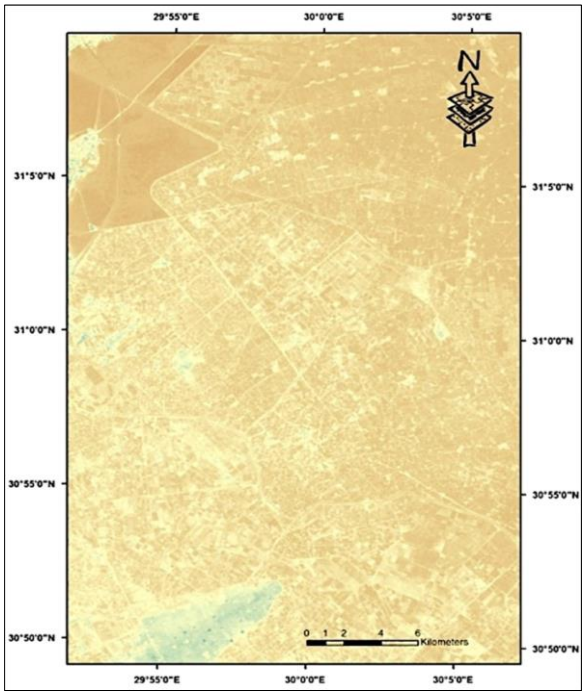

Figure 7. Landsat 5 TM image of the first study area

For validation purposes, the ground reference datasets corresponding to each study area are presented separately. The reference data for the first study area (JICA, 1995) include EC measurements of soil samples collected at depths ⩽ 0.5 m (see Figure 8) [47].

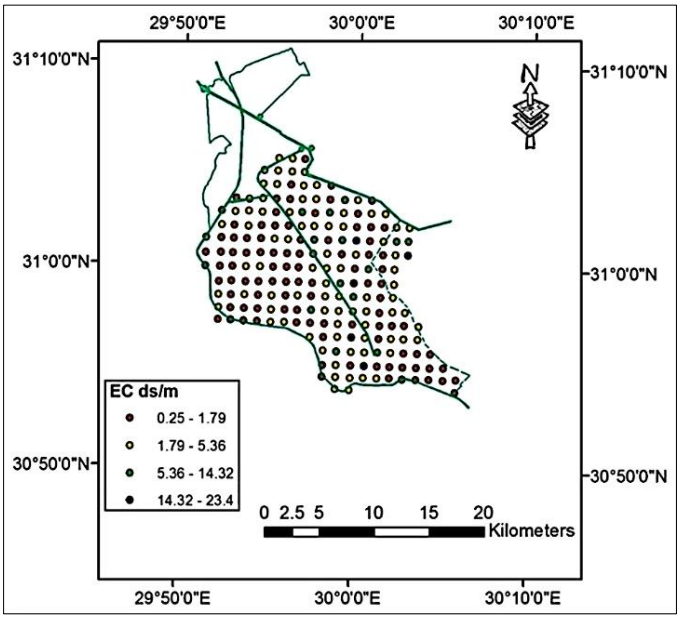

Figure 8. Spatial distribution of reference soil samples for the first study area

The reference data for the second study area consist of TDS measurements from soil samples collected at approximately 1 m depth along the Mansoura–Damietta railway corridor (Figure 9).

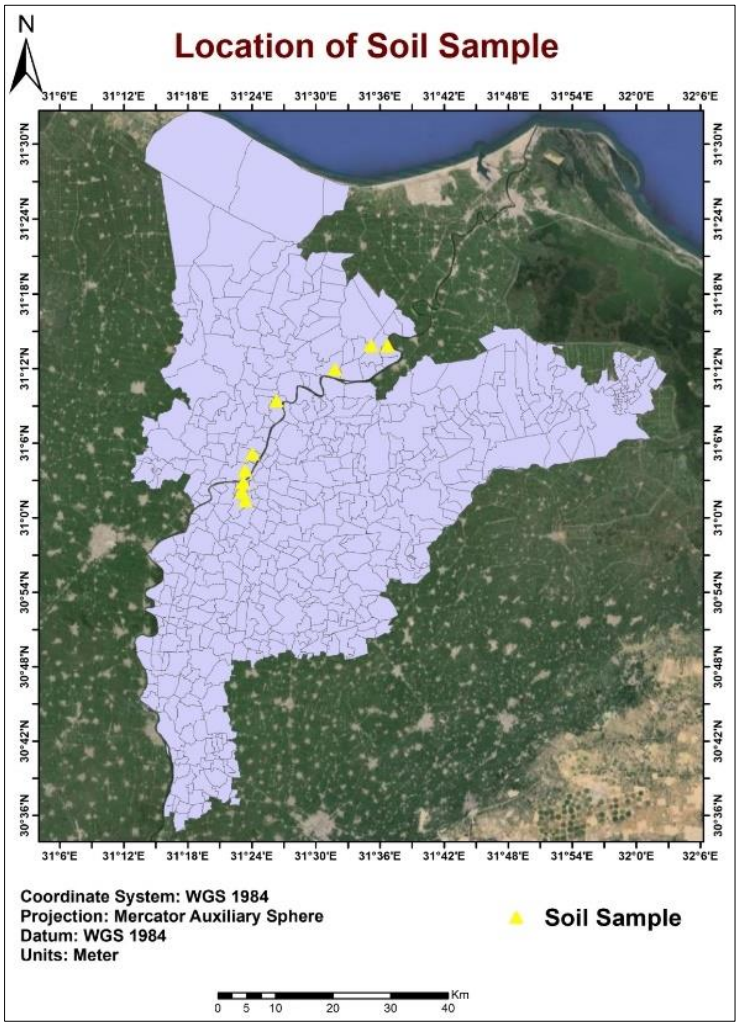

Figure 9. Spatial distribution of reference soil samples for the second study area

3. Methodology

The methodological framework adopted in this study follows a structured workflow consisting of four main stages: image preprocessing, spectral processing, post-processing, and comparative analysis. A schematic overview of the workflow is presented in Figure 10. The use of different software platforms (SNAP for Sentinel-2 and ATCOR for Landsat) was based on sensor-specific optimization, ensuring accurate atmospheric correction tailored to each satellite system.

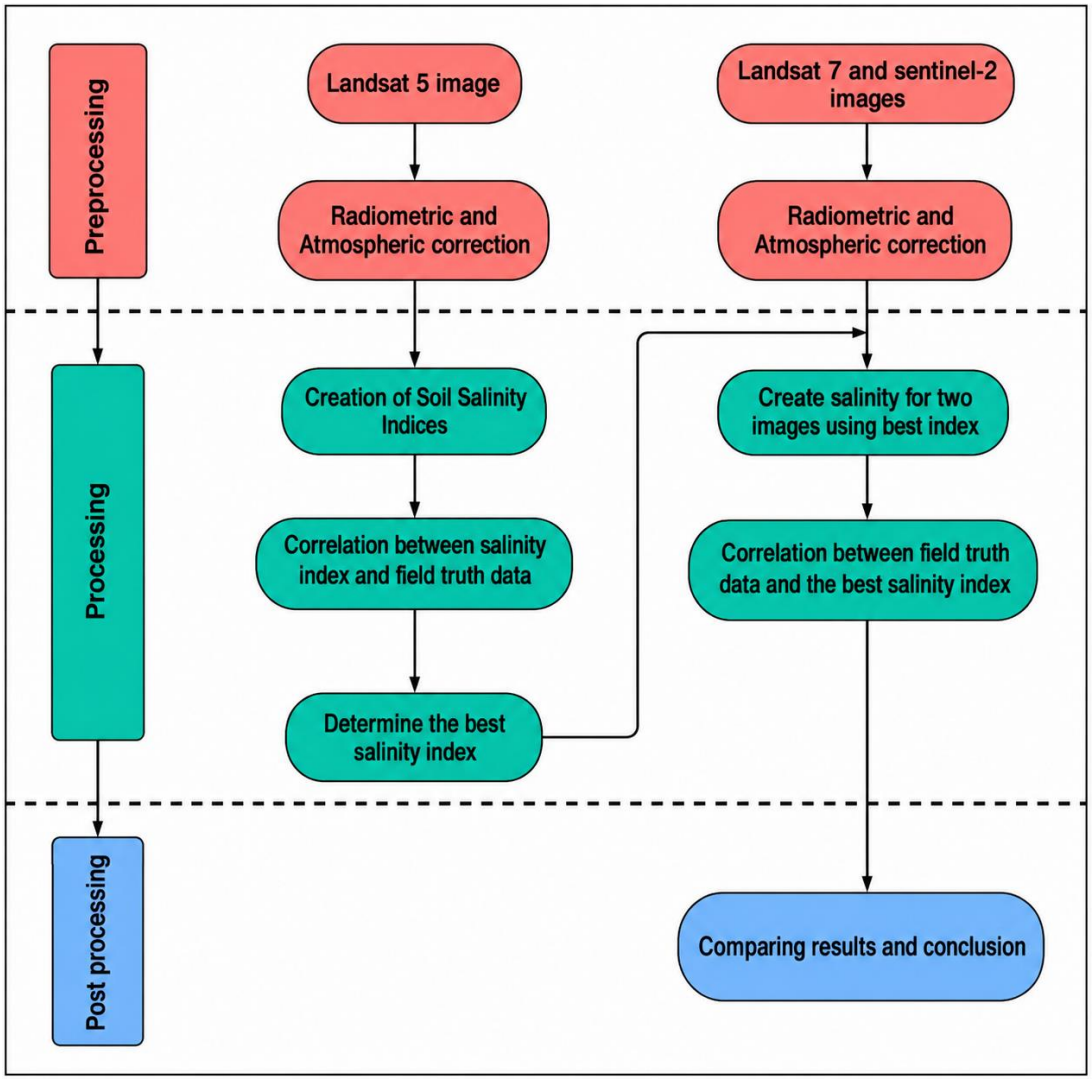

Figure 10. Schematic diagram of the methodological workflow adopted in this study

3.1. Image Preprocessing

The preprocessing stage involved the integration of satellite imagery and ground-based measurements to ensure spatial consistency and radiometric reliability. The satellite datasets, including Sentinel-2, Landsat 5 TM, and Landsat 7 ETM+, were subjected to radiometric calibration and atmospheric correction to derive surface reflectance values suitable for quantitative analysis. Radiometric calibration was first applied to convert raw digital numbers into physically meaningful radiance values. Subsequently, atmospheric correction was performed to remove atmospheric effects and retrieve bottom-of-atmosphere reflectance, which is essential for accurate spectral analysis in arid environments [48].

Sentinel-2 imagery was processed using the SNAP platform, employing standard atmospheric correction procedures to generate Level-2A surface reflectance products. Landsat 5 and Landsat 7 datasets were processed using the ATCOR module, which applies radiative transfer-based correction to account for atmospheric scattering and absorption effects. All corrected images were geometrically aligned and projected to the WGS 84 / UTM Zone 36N coordinate system. The outputs of the preprocessing stage are illustrated in Figures 11 to 13.

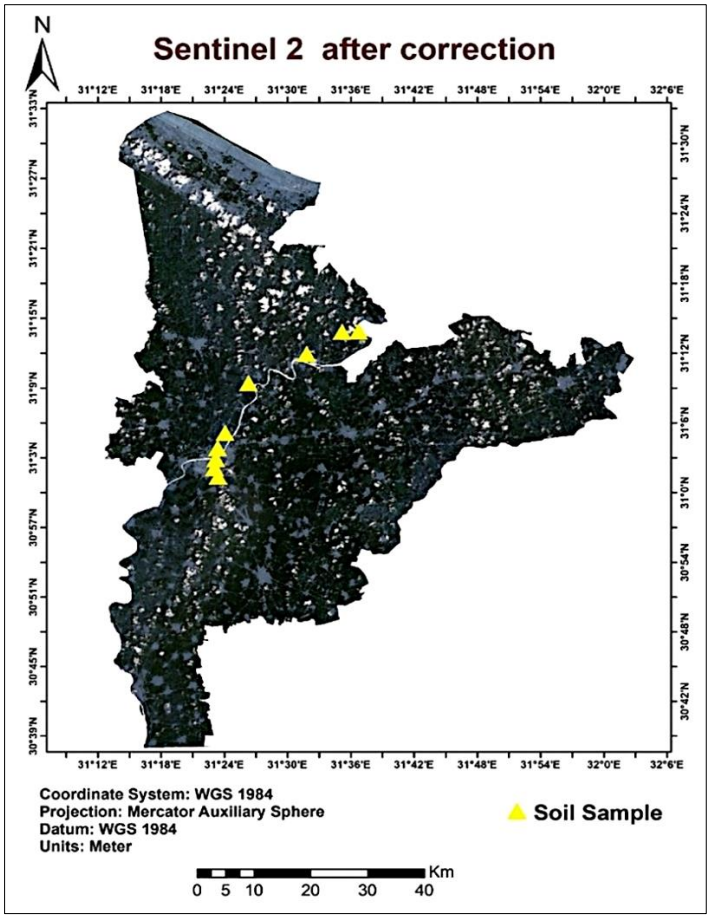

Figure 11. Sentinel-2 surface reflectance image after atmospheric correction

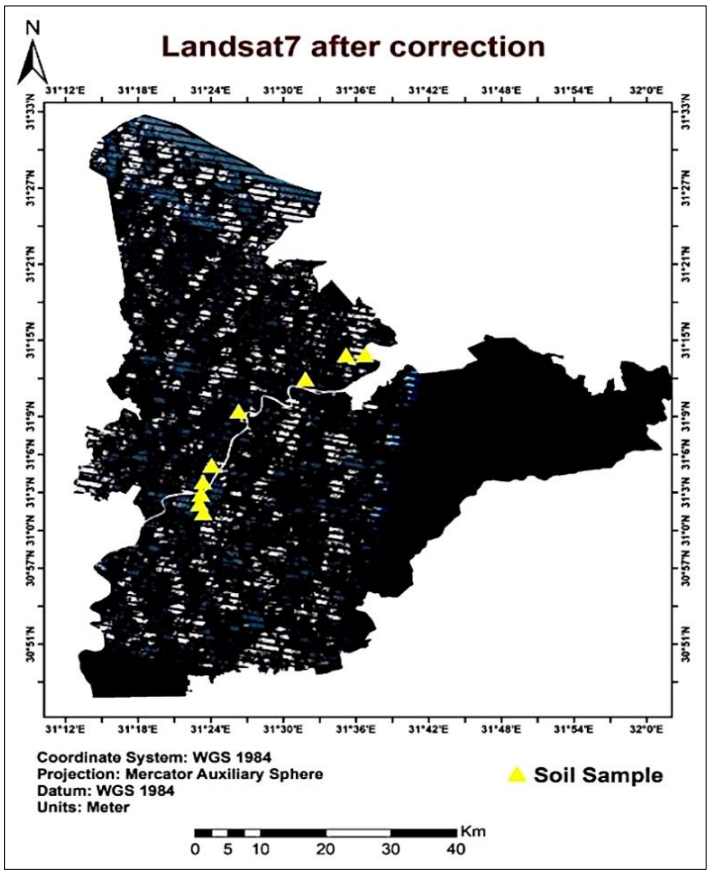

Figure 12. Landsat 7 ETM+ surface reflectance image after correction

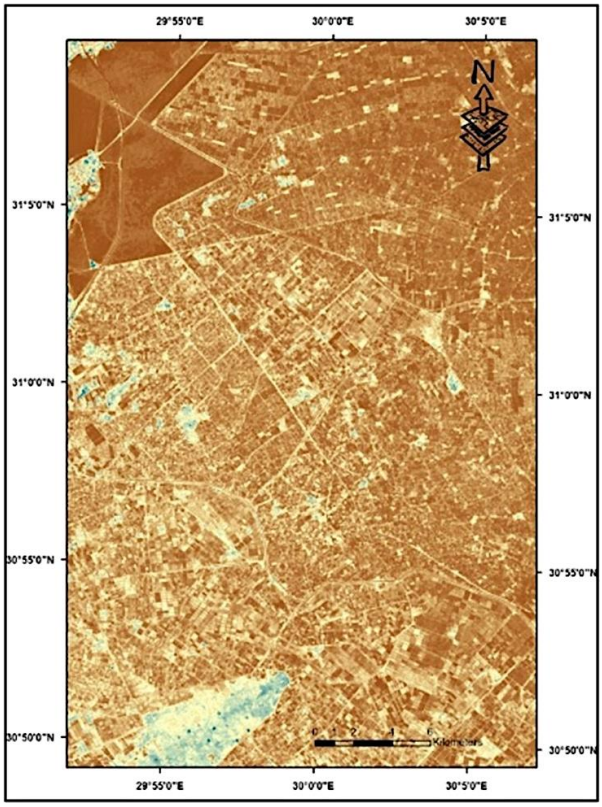

Figure 13. Landsat 5 TM surface reflectance image after correction

3.2. Spectral Processing and Salinity Index Evaluation

Following preprocessing, spectral salinity indices were derived from the Landsat 5 imagery to establish a calibration baseline. A total of seven salinity indices, previously reported in the literature, were computed using surface reflectance values. To evaluate the performance of these indices, a linear regression analysis was conducted between the spectral index values and corresponding in-situ soil salinity measurements. The relationship was assessed using the correlation coefficient (r) and the coefficient of determination (R^2).

The results of this analysis are summarized in Table 1, which presents the mathematical expressions of the indices along with their statistical performance. Among the evaluated indices, Salinity Index 5 (SI5) exhibited the strongest correlation with field measurements and was therefore selected as the most suitable indicator for subsequent analysis.

Table 1. Mathematical formulations and statistical performance of evaluated salinity indices based on Landsat 5 calibration

Modelling Indices	Acronym	Equation	Reference	Correlation	R^2	Mean RE (%)
Salinity index 1	SI1	$(G \times R)^{0.5}$	Douaoui et al. [49]	0.232	0.054	87.8
Salinity index 2	SI2	$(B \times R)^{0.5}$	Khan et al. [50]	0.228	0.052	96.9
Salinity index 3	SI3	(B − R) / (B + R)	Bannari et al. [51]	0.133	0.018	113.6
Salinity index 4	SI4	NIR / R	Major et al. [52]	0.452	0.204	43.2
Salinity index 5	SI5	(R × NIR) / G	Abbas & Khan [53]	0.870	0.762	22.7
Salinity index 6	SI6	(B × R) / G	Abbas & Khan [53]	0.340	0.121	65.3
Normalized difference salinity index	NDSI	(R − NIR) / (R + NIR)	Khan et al. [54]	-0.452	0.205	45.6

3.3. Image Postprocessing

Salinity index images were created, and their salinity values in surface reflectance (SR) were extracted for both satellite images. These values were then compared with the field-truth TDS data at specific points. The corresponding SR-based index values were extracted at locations coinciding with the ground sampling points.

These extracted values were then compared with the field-measured Total Dissolved Solids (TDS) data. A statistical analysis was performed to quantify the relationship between the remotely sensed salinity index and in-situ measurements using Simple Linear Regression (SLR). This step enabled the evaluation of the predictive capability of the selected index and provided a basis for model validation.

4. Results

Based on the statistical evaluation of the candidate salinity indices (Table 1), Salinity Index 5 (SI5) demonstrated the strongest correlation with field measurements and was therefore selected for subsequent analysis. Using this index, spatial distribution maps of soil salinity were generated from both Landsat 7 and Sentinel-2 imagery, as shown in Figure 14.

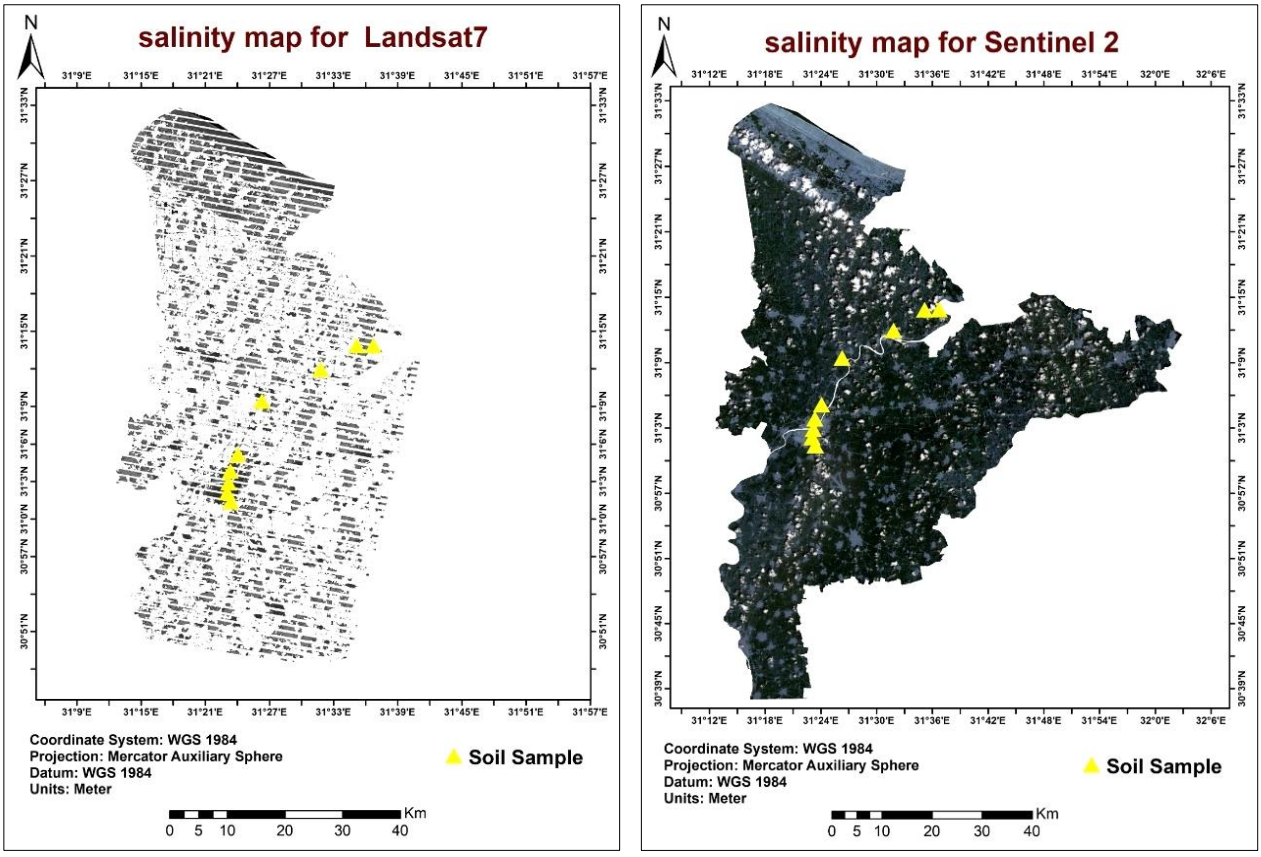

Figure 14. Spatial distribution of soil salinity derived from Landsat 7 and Sentinel-2 imagery using SI5

To assess the accuracy of satellite-derived salinity estimates, index values were extracted at locations corresponding to field sampling points. The relationship between the spectral index and measured TDS values was analyzed using Simple Linear Regression (SLR), with results presented in Figure 15.

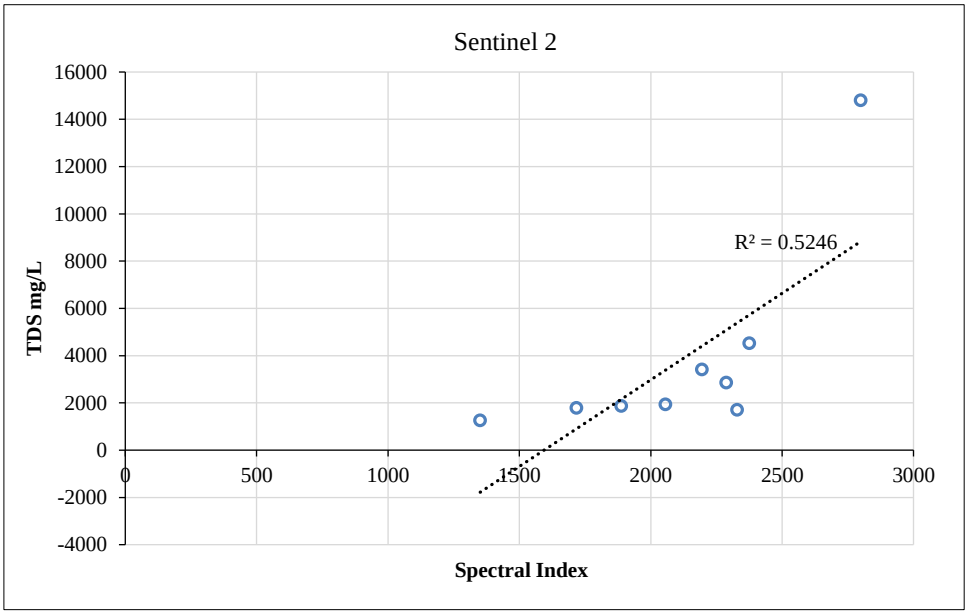

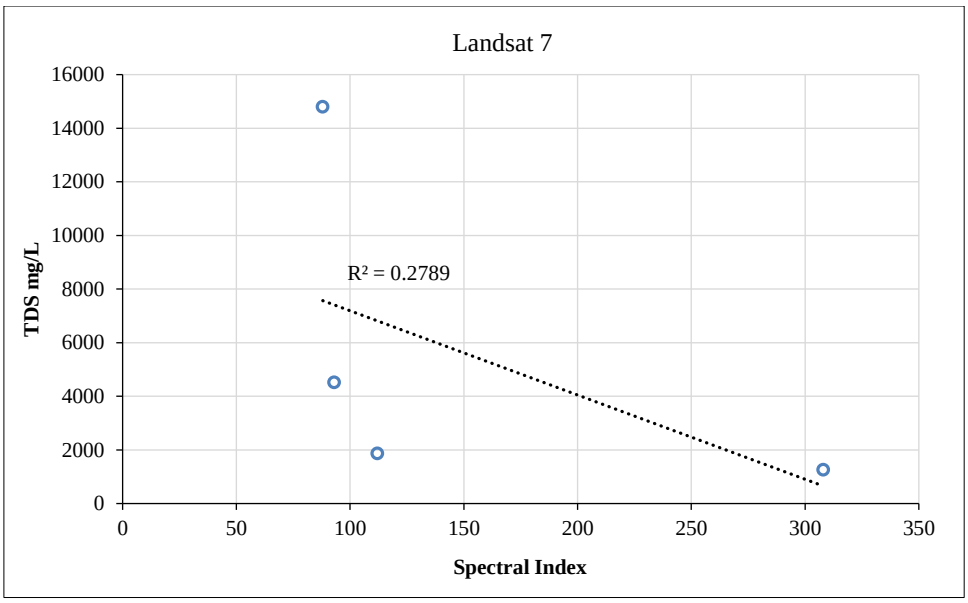

Figure 15. Linear relationship between field-measured TDS and spectral salinity index values derived from Landsat 7 and Sentinel-2

The results indicate a strong correlation between remotely sensed spectral responses and soil salinity levels. This finding is consistent with previous studies demonstrating that soil reflectance is influenced by key properties such as moisture content, mineral composition, and salt concentration [55-57]. In particular, multispectral data from Sentinel-2 have been shown to provide enhanced sensitivity to salinity variations due to their higher spatial and spectral resolution [58].

A comparative analysis between Landsat 7 and Sentinel-2 revealed that Sentinel-2 generally provides improved predictive performance, likely due to its finer spatial resolution (10 m) and additional spectral bands. However, Landsat 7 remains valuable for long-term monitoring due to its historical data continuity.

To further refine the estimation of soil salinity, multiple regression models of varying complexity, including linear, polynomial, and exponential functions, were evaluated. The performance of these models was assessed using correlation coefficients and relative error (RE%). The results of this comparative evaluation are summarized in Table 2. The negative correlation observed for Landsat 7 ($r = -0.52$) indicates an inverse relationship; however, the magnitude of correlation ($|r|$) is used to assess strength. While the corresponding regression relationships are illustrated in Figures 16 and 17.

Table 2. Performance comparison of salinity estimation models derived from Landsat 7 and Sentinel-2 imagery

Index	Sentinel-2	Landsat 7
Correlation	0.72	-0.52
Mean RE (%)	36	48
R^2 (1st degree equation)	0.52	0.28
R^2 (2nd degree equation)	0.89	0.72
R^2 (Exponential equation)	0.69	0.49

Following the evaluation of multiple regression models, second-degree polynomial functions demonstrated superior performance in representing the relationship between spectral salinity indices and field-measured salinity. Compared to linear and higher-order models, the quadratic models provided the best fit to the observed data, effectively capturing the non-linear behavior of salinity variation.

The fitted polynomial curves exhibited strong agreement with the ground truth measurements, closely reproducing both the increasing and decreasing trends in salinity levels. This is reflected in the high coefficients of determination, with $R^2 = 0.89$ for Sentinel-2 and $R^2 = 0.72$ for Landsat 7, indicating a robust predictive capability.

The improved performance of the quadratic model suggests that soil salinity–spectral relationships in the study areas are inherently non-linear, likely due to the combined effects of soil moisture, texture, and salt concentration on spectral reflectance. Consequently, second-degree polynomial models are recommended for salinity prediction in similar arid and semi-arid environments, where such non-linear interactions are prevalent.

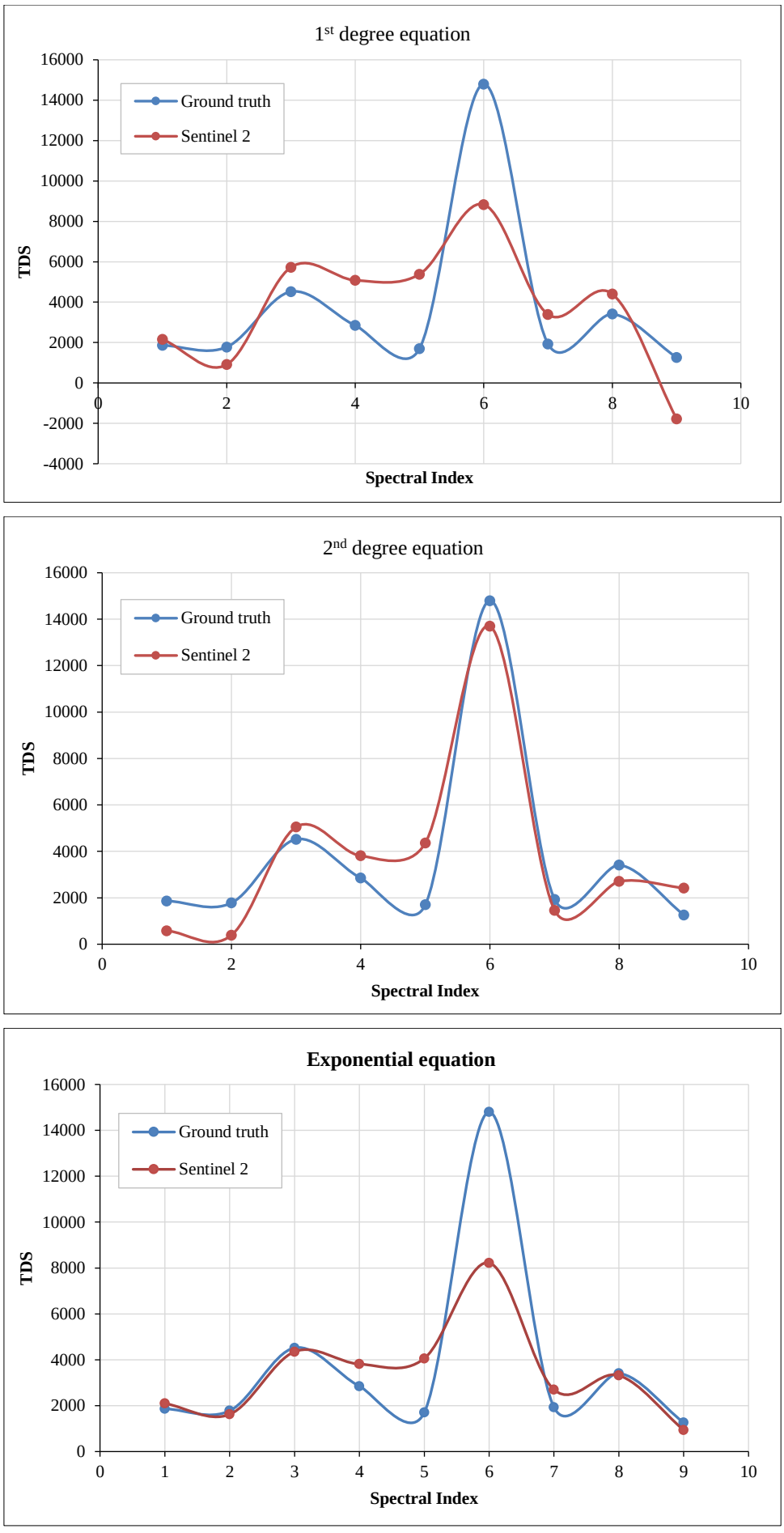

Figure 16. Sentinel-2 salinity index compared to field data using different equation degrees

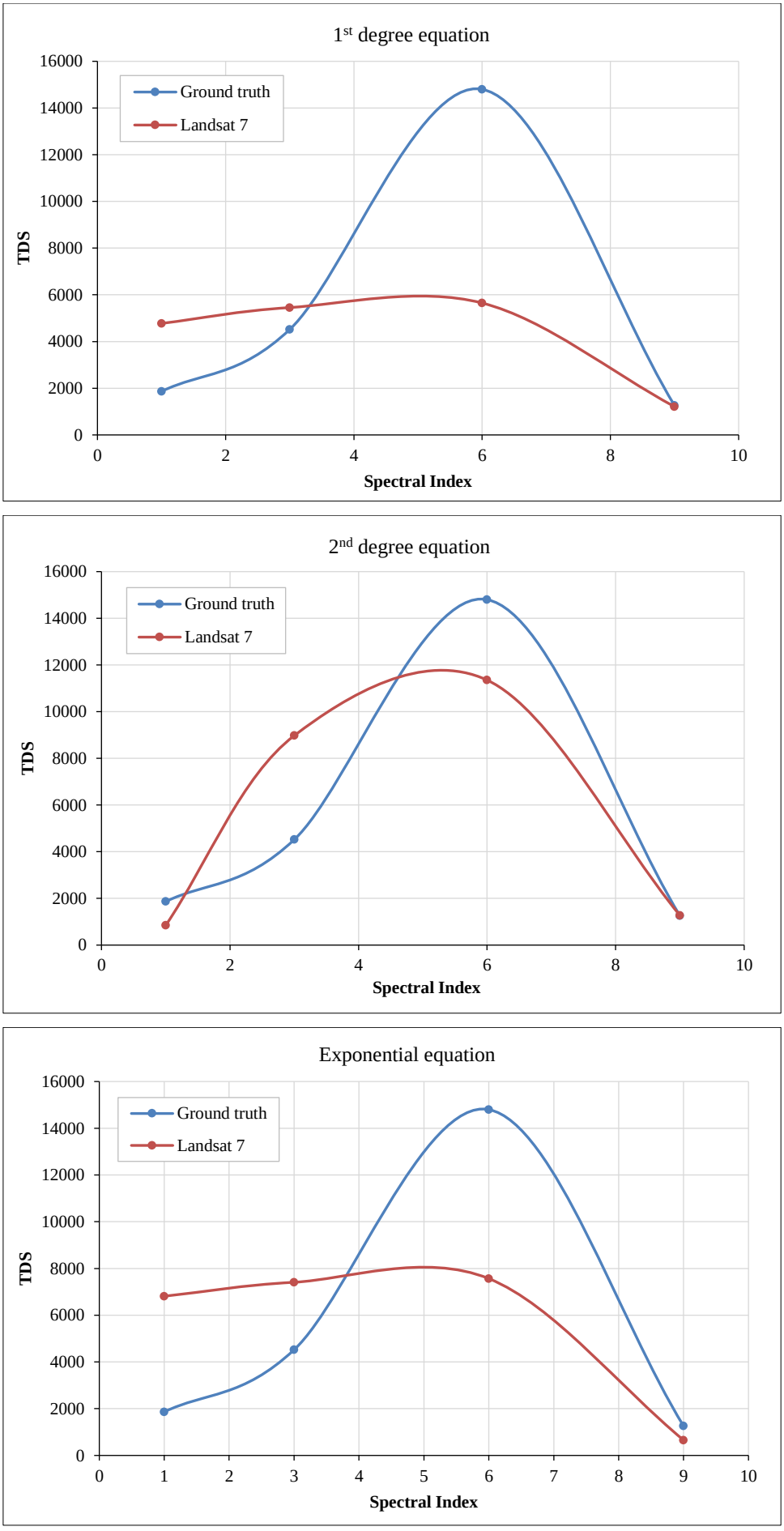

Figure 17. Landsat 7 salinity index compared to field data using different equation degrees

5. Discussion

Soil salinization represents a major threat to agricultural productivity and environmental sustainability, particularly in arid and semi-arid regions such as Egypt [59, 60]. In the Nile Delta, this issue is exacerbated by shallow groundwater, intensive irrigation practices, and poor drainage conditions, which collectively promote salt accumulation in the root zone. Within this context, remote sensing offers a scalable and cost-effective approach for monitoring salinity dynamics; however, its effectiveness depends strongly on sensor characteristics and modeling strategies.

This study provides a comprehensive evaluation of the combined effects of sensor spatial resolution, spectral index selection, and regression modeling on soil salinity estimation, with a particular focus on subsurface salinity detection. It should be noted that the limited number of field samples in the second study area represents a constraint, and future studies should incorporate higher sampling density to improve statistical robustness.

Recent studies published in 2026 further confirm the effectiveness of Sentinel-2 data for soil salinity mapping, particularly when combined with advanced modeling techniques. For instance, machine learning-based approaches applied to Sentinel-2 imagery have achieved high predictive performance ($R^2 \approx 0.87$), demonstrating their superiority over traditional regression methods in capturing complex soil–spectral relationships [61]. In addition, recent review studies highlight that current research trends are increasingly focused on integrating multi-source, multi-scale remote sensing data with artificial intelligence to improve salinity monitoring accuracy and scalability [62]. These developments strongly support the findings of the present study, where high-resolution Sentinel-2 data and non-linear modeling approaches significantly improved salinity estimation accuracy.

5.1. Impact of Sensor Spatial Resolution

The transition from Landsat sensors (30 m resolution) to Sentinel-2 MSI (10 m resolution) represents a significant advancement in the capability to monitor soil salinity at finer spatial scales. In heterogeneous agricultural landscapes such as the Nile Delta, Landsat pixels often represent mixed signals from soil, vegetation, irrigation channels, and salt crusts, leading to reduced accuracy in salinity estimation.

In contrast, Sentinel-2 significantly reduces mixed-pixel effects, enabling improved detection of localized salinity features, including narrow salt-affected zones along drainage networks. This improvement is reflected in the present study, where Sentinel-2 achieved higher predictive performance ($R^2 = 0.89$) compared to Landsat 7 ($R^2 = 0.72$).

These findings are consistent with previous studies demonstrating that higher spatial resolution enhances salinity mapping accuracy by minimizing spectral mixing and improving the delineation of small-scale variability [40, 63, 64].

5.2. Performance of Spectral Salinity Indices

Spectral salinity indices exploit the distinct reflectance properties of salt-affected soils, particularly in the visible, near-infrared (NIR), and shortwave infrared (SWIR) regions. However, their performance is strongly influenced by soil texture, moisture content, and vegetation cover.

In this study, Salinity Index 5 (SI5) was identified as the most effective predictor, achieving strong agreement with field measurements. The formulation of SI5 allows it to capture both increased reflectance from salt crusts and variations in soil background, making it particularly suitable for clay-rich alluvial soils.

This finding aligns with studies conducted in similar environments, where SI5 demonstrated high predictive capability (e.g., $R^2 > 0.9$ in semi-arid regions) [65, 66]. However, the literature also highlights regional variability in index performance. For example, in calcareous or vegetated environments, indices such as SI2 or VSSI may outperform SI5 due to reduced sensitivity to vegetation interference.

These discrepancies emphasize that no single spectral index is universally optimal, and index selection should be adapted to local soil and land-use conditions.

5.3. Non-Linearity in Soil Salinity Modeling

A key finding of this study is the superiority of second-degree polynomial models over linear regression for salinity estimation. The relationship between spectral response and soil salinity is inherently non-linear, influenced by factors such as reflectance saturation at high salt concentrations and interactions with soil moisture.

The adoption of quadratic models resulted in a substantial improvement in predictive performance, increasing R^2 values from 0.52 to 0.89 for Sentinel-2 and from 0.28 to 0.72 for Landsat 7. These results demonstrate that polynomial models are better suited to capturing the complex spectral behavior of saline soils across a wide range of salinity levels [5, 40, 41, 67-69].

This finding is consistent with previous research, which shows that linear models tend to underestimate high salinity and overestimate low salinity, whereas non-linear approaches provide more balanced predictions across the full range of conditions.

5.4. Comparative Analysis with Regional and Global Studies

The results of this study are broadly consistent with findings from both regional and international research, while also highlighting important context-specific variations. First, the identification of SI5 as the optimal index contrasts with studies in other Egyptian regions, where indices such as SI2 or SI7 have shown higher accuracy. This variation reflects differences in soil composition, particularly between clay-rich deltaic soils and calcareous desert environments. Second, the superior performance of Sentinel-2 over Landsat aligns with international studies, including Davis (2018) [40], which reported improved salinity mapping accuracy due to reduced mixed-pixel effects at higher spatial resolution. Third, the demonstrated advantage of polynomial modeling is supported by multiple studies, which consistently show that second-order models provide better predictive accuracy in semi-arid environments due to their ability to capture non-linear spectral responses. Overall, these comparisons confirm that sensor resolution, index selection, and modeling approach must be jointly optimized to achieve reliable salinity estimation.

5.5. Subsurface Salinity Detection

The ability to infer subsurface salinity from surface spectral data remains a major challenge in remote sensing. In this study, a strong correlation ($R^2 = 0.89$) was observed between Sentinel-2-derived indices and salinity measurements at depths up to 1 m [30, 57, 59].

This result suggests that, under certain conditions, surface reflectance can serve as a proxy for subsurface salinity due to vertical hydrological connectivity in alluvial soils. However, previous studies indicate that prediction accuracy generally decreases with depth, particularly in the absence of auxiliary variables such as topography or soil moisture [70]. Therefore, while the results are promising, the use of optical remote sensing for subsurface salinity detection should be interpreted with caution and ideally supported by additional data sources.

The findings of this study demonstrate that the integration of high-resolution satellite data (Sentinel-2), robust spectral indices (SI5), and non-linear modeling approaches provide a reliable framework for soil salinity assessment in arid environments. Future research should focus on (1) incorporating machine learning models to further improve predictive accuracy, (2) integrating multi-source data (e.g., SAR, topography, soil moisture), and (3) expanding validation datasets to include deeper soil profiles and temporal variability. Such advancements will enhance the capability of remote sensing to support sustainable land and water management in salinity-affected regions.

6. Conclusions

Soil salinization represents a critical environmental challenge, particularly in arid and semi-arid regions such as Egypt, where hydrological and climatic conditions accelerate salt accumulation in agricultural lands. This study demonstrates the effectiveness of integrating remote sensing (RS), GIS, and ground-based measurements for the spatial assessment and modeling of soil salinity.

The results confirm that spectral salinity indices derived from multispectral satellite data provide a reliable means for mapping salinity distribution. Among the evaluated indices, Salinity Index 5 (SI5) exhibited the strongest correlation with field measurements and was therefore selected as the most suitable indicator for salinity assessment in the study areas. A key finding of this research is the significant influence of sensor spatial resolution on salinity retrieval accuracy. Sentinel-2 imagery (10 m) outperformed Landsat 7 (30 m), achieving a higher coefficient of determination ($R^2 = 0.89$) compared to Landsat 7 ($R^2 = 0.72$). This improvement is attributed to the reduced mixed-pixel effect and enhanced ability to capture fine-scale spatial variability in heterogeneous agricultural landscapes.

Furthermore, the study highlights the importance of non-linear modeling approaches. Second-degree polynomial regression demonstrated superior performance over linear models, effectively capturing the complex relationship between spectral response and soil salinity. This confirms that salinity–spectral relationships are inherently non-linear and require appropriate modeling strategies to improve prediction accuracy. Importantly, the results indicate that remote sensing-based indices can provide meaningful estimates of subsurface salinity (up to ~1 m depth) under certain environmental conditions, likely due to hydrological connectivity between surface and root-zone processes. However, this capability remains context-dependent and should be interpreted with caution. Overall, the integration of high-resolution satellite data, robust spectral indices, and non-linear modeling offers a reliable and scalable framework for soil salinity monitoring in arid environments. This approach supports more efficient land management and decision-making processes in salinity-affected regions.

Future research should focus on: (1) incorporating machine learning techniques to further enhance prediction accuracy, (2) integrating multi-source datasets (e.g., SAR, soil moisture, topography), (3) expanding validation across different soil types and climatic conditions, and (4) investigating the limits of subsurface salinity detection using optical sensors. Such advancements will strengthen the applicability of remote sensing for sustainable agricultural management and environmental monitoring in salinity-prone regions.

7. List of Abbreviation

Abbreviation	Definition	Abbreviation	Definition
ATCOR	Atmospheric and Topographic Correction	DN	Digital Number
EC	Electrical Conductivity	ETM+	Enhanced Thematic Mapper Plus
GIS	Geographic Information System	GNSS	Global Navigation Satellite System
JICA	Japan International Cooperation Agency	MSI	Multispectral Instrument
NDSI	Normalized Difference Salinity Index	NIR	Near-Infrared
RE (%)	Relative Error (%)	RS	Remote Sensing
SI	Salinity Index	SI1	Salinity Index 1
SI2	Salinity Index 2	SI3	Salinity Index 3
SI4	Salinity Index 4	SI5	Salinity Index 5
SI6	Salinity Index 6	SNAP	Sentinel Application Platform
SLR	Simple Linear Regression	SR	Surface Reflectance
SWIR	Shortwave Infrared	TDS	Total Dissolved Solids
TM	Thematic Mapper	UTM	Universal Transverse Mercator
WGS 84	World Geodetic System 1984		

8. Declarations

8.1. Author Contributions

Conceptualization, M.E. and M.G.; methodology, M.G. and M.R.; software, M.E., M.M., and M.G.; validation, M.M., M.F., and M.R.; formal analysis, M.E., M.M., M.G., and M.R.; investigation, M.E., M.G., and M.R.; resources, M.F. and M.R.; data curation, M.E., M.G., and M.R.; writing—original draft preparation, M.E., M.G., and M.R.; writing—review and editing, M.F. and M.R.; visualization, M.E., M.M., and M.G.; supervision, M.F. and M.R.; project administration, M.F.; funding acquisition, M.F. All authors have read and agreed to the published version of the manuscript.

8.2. Data Availability Statement

The data presented in this study are available on request from the corresponding author.

8.3. Funding

This research was funded by the UAE University grant number 12N264.

8.4. Acknowledgments

The authors acknowledge the open-access data provided by the Landsat 5 and 7 missions and the Sentinel-2 satellites. The authors also acknowledge the Japan International Cooperation Agency (JICA) and Arab Consulting Engineers (ACE) for providing ground-truth and in situ data.

8.5. Conflicts of Interest

The authors declare no conflict of interest.

9. References

[1] Chen, H., Ma, Y., Zhu, A., Wang, Z., Zhao, G., & Wei, Y. (2021). Soil salinity inversion based on differentiated fusion of satellite image and ground spectra. International Journal of Applied Earth Observation and Geoinformation, 101, 102360. doi:10.1016/j.jag.2021.102360.

[2] Lotfollahi, L., Delavar, M. A., Biswas, A., Fatehi, S., & Scholten, T. (2023). Spectral prediction of soil salinity and alkalinity indicators using visible, near-, and mid-infrared spectroscopy. Journal of Environmental Management, 345, 118854. doi:10.1016/j.jenvman.2023.118854.

[3] Seifi, M., Ahmadi, A., Neyshabouri, M. R., Taghizadeh-Mehrjardi, R., & Bahrami, H. A. (2020). Remote and Vis-NIR spectra sensing potential for soil salinization estimation in the eastern coast of Urmia hyper saline lake, Iran. Remote Sensing Applications: Society and Environment, 20, 100398. doi:10.1016/j.rsase.2020.100398.

[4] Zarei, A., Hasanlou, M., & Mahdianpari, M. (2021). A comparison of machine learning models for soil salinity estimation using multi-spectral earth observation data. ISPRS Annals of the Photogrammetry, Remote Sensing and Spatial Information Sciences, V-3-2021, 257–263. doi:10.5194/isprs-annals-V-3-2021-257-2021.

[5] Fadl, M. E., Jalhoum, M. E. M., AbdelRahman, M. A. E., Ali, E. A., Zahra, W. R., Abuzaid, A. S., Fiorentino, C., D'Antonio, P., Belal, A. A., & Scopa, A. (2023). Soil Salinity Assessing and Mapping Using Several Statistical and Distribution Techniques in Arid and Semi-Arid Ecosystems, Egypt. Agronomy, 13(2), 583. doi:10.3390/agronomy13020583.

[6] Xu, X., Chen, Y., Wang, M., Wang, S., Li, K., & Li, Y. (2021). Improving estimates of soil salt content by using two-date image spectral changes in yinbei, china. Remote Sensing, 13(20), 4165. doi:10.3390/rs13204165.

[7] Hillel, D. (2000). Salinity management for sustainable irrigation: Integrating science, environment, and economics: The World Bank, Washington, DC, United States. doi:10.1596/0-8213-4773-x.

[8] Negacz, K., Malek, Ž., de Vos, A., & Vellinga, P. (2022). Saline soils worldwide: Identifying the most promising areas for saline agriculture. Journal of Arid Environments, 203, 104775. doi:10.1016/j.jaridenv.2022.104775.

[9] Wang, N., Chen, S., Huang, J., Frappart, F., Taghizadeh, R., Zhang, X., Wigneron, J. P., Xue, J., Xiao, Y., Peng, J., & Shi, Z. (2024). Global Soil Salinity Estimation at 10 m Using Multi-Source Remote Sensing. Journal of Remote Sensing (United States), 4, 130. doi:10.34133/remotesensing.0130.

[10] Aboelsoud, H. M., AbdelRahman, M. A. E., Kheir, A. M. S., Eid, M. S. M., Ammar, K. A., Khalifa, T. H., & Scopa, A. (2022). Quantitative Estimation of Saline-Soil Amelioration Using Remote-Sensing Indices in Arid Land for Better Management. Land, 11(7), 1041. doi:10.3390/land11071041.

[11] Aboelsoud, H. M., Habib, A., Engel, B., Hashem, A. A., El-Hassan, W. A., Govind, A., Elnashar, A., Eid, M., & Kheir, A. M. S. (2023). The combined impact of shallow groundwater and soil salinity on evapotranspiration using remote sensing in an agricultural alluvial setting. Journal of Hydrology: Regional Studies, 47, 101372. doi:10.1016/j.ejrh.2023.101372.

[12] Gorji, T., Tanik, A., & Sertel, E. (2015). Soil Salinity Prediction, Monitoring and Mapping Using Modern Technologies. Procedia Earth and Planetary Science, 15, 507–512. doi:10.1016/j.proeps.2015.08.062.

[13] Wang, J., Ding, J., Yu, D., Teng, D., He, B., Chen, X., Ge, X., Zhang, Z., Wang, Y., Yang, X., Shi, T., & Su, F. (2020). Machine learning-based detection of soil salinity in an arid desert region, Northwest China: A comparison between Landsat-8 OLI and Sentinel-2 MSI. Science of the Total Environment, 707, 136092. doi:10.1016/j.scitotenv.2019.136092.

[14] Dwivedi, R. S., Sreenivas, K., & Ramana, K. V. (1999). Inventory of salt-affected soils and waterlogged areas: A remote sensing approach. International Journal of Remote Sensing, 20(8), 1589–1599. doi:10.1080/014311699212623.

[15] Metternicht, G. I., & Zinck, J. A. (2003). Remote sensing of soil salinity: Potentials and constraints. Remote Sensing of Environment, 85(1), 1–20. doi:10.1016/S0034-4257(02)00188-8.

[16] Freeshah, M., Osama, N., & Zhang, X. (2023). Using real GNSS data for ionospheric disturbance remote sensing associated with strong thunderstorm over Wuhan city. Acta Geodaetica et Geophysica, 58(4), 553–574. doi:10.1007/s40328-023-00423-w.

[17] Saqib, M., Şentürk, E., Arqim Adil, M., & Freeshah, M. (2024). Seismo-ionospheric precursory detection using hybrid Bayesian-LSTM network model with uncertainty-boundaries and anomaly-intensity. Advances in Space Research, 74(4), 1828–1842. doi:10.1016/j.asr.2024.05.023.

[18] Freeshah, M., Adil, M. A., Şentürk, E., Zhang, X., Ren, X., Liu, H., & Osama, N. (2024). A cyclone formation, eastward plume drag, ion-hydration process, and the consequent ionospheric changes following the 2022 Hunga Tonga-Hunga Ha'apai volcanic eruption. Advances in Space Research, 73(5), 2457–2470. doi:10.1016/j.asr.2023.12.029.

[19] Freeshah, M., Şentürk, E., Zhang, X., Livaoğlu, H., Ren, X., & Osama, N. (2024). Investigating Multiple Ionospheric Disturbances Associated with the 2020 August 4 Beirut Explosion by Geodetic and Seismological Data. Pure and Applied Geophysics, 181(3), 875–894. doi:10.1007/s00024-023-03386-9.

[20] Fathy, A., Otsuka, Y., Ghamry, E., Marchetti, D., Pradipta, R., Farid, A. I. S., & Freeshah, M. (2025). Insights into Conjugate Hemispheric Ionospheric Disturbances Associated with the Beirut Port Explosion on 4 August 2020 Using Multi Low-Earth-Orbit Satellites. Remote Sensing, 17(11), 1908. doi:10.3390/rs17111908.

[21] Cheng, J., Zhang, X., Zhu, F., Hu, J., Zhuo, D., & Freeshah, M. (2025). A tightly coupled integration of GNSS/IMU/LiDAR with parameterized semantic line and plane features to improve pose accuracy in complex environments. Measurement, 247, 116843. doi:10.1016/j.measurement.2025.116843.

[22] Elshewy, M. A., Trung Thanh, P., Elsheshtawy, A. M., Refaat, M., & Freeshah, M. (2024). A novel approach for optimizing regional geoid modeling over rugged terrains based on global geopotential models and artificial intelligence algorithms. Egyptian Journal of Remote Sensing and Space Science, 27(4), 656–668. doi:10.1016/j.ejrs.2024.09.002.

[23] Mehrjardi, R. T., Mahmoodi, S. H., Taze, M., & Sahebjalal, E. (2008). Accuracy assessment of soil salinity map in Yazd-Ardakan Plain, Central Iran, based on Landsat ETM+ imagery. American-Eurasian Journal of Agricultural & Environmental Sciences, 3(5), 708-712.

[24] Dwivedi, R. S. (2001). Soil resources mapping: A remote sensing perspective. Remote Sensing Reviews, 20(2), 89–122. doi:10.1080/02757250109532430.

[25] Lizaga, I., Quijano, L., Gaspar, L., Ramos, M. C., & Navas, A. (2019). Linking land use changes to variation in soil properties in a Mediterranean mountain agroecosystem. Catena, 172, 516–527. doi:10.1016/j.catena.2018.09.019.

[26] Santra, P., Singh, R., Sarathjith, M. C., Panwar, N. R., Varghese, P., & Das, B. S. (2015). Reflectance spectroscopic approach for estimation of soil properties in hot arid western Rajasthan, India. Environmental Earth Sciences, 74(5), 4233–4245. doi:10.1007/s12665-015-4383-x.

[27] Madrigal, L. P., Wiegand, C. L., Meraz, J. G., Rubio, B. D. R., Estrada, X. C., & Ramirez, O. L. (2003). Soil salinity and its effect on crop yield-a study using satellite imagery in three irrigation districts. Ingenieria Hidraulica en Mexico, 18(2), 83-97.

[28] Diana, N. A., Soemitro, R. A. A., Ekaputri, J. J., Satrya, T. R., & Warnana, D. D. (2025). Dynamic Analysis of MICP-Stabilized Soil and Liquefiable Soil with Varying Salinity Levels. Civil Engineering Journal, 11(4), 1432–1446. doi:10.28991/CEJ-2025-011-04-010.

[29] Farifteh, J. (2007). Imaging spectroscopy of salt-affected soils: Model-based integrated method. Ph.D. Thesis, Utrecht University, Utrecht, Netherlands.

[30] Ranjbar, S., Zarei, A., Hasanlou, M., Akhoondzadeh, M., Amini, J., & Amani, M. (2021). Machine learning inversion approach for soil parameters estimation over vegetated agricultural areas using a combination of water cloud model and calibrated integral equation model. Journal of Applied Remote Sensing, 15(1), 17. doi:10.1117/1.jrs.15.018503.

[31] Teggi, S., Costanzini, S., Despini, F., Chiodi, P., & Immordino, F. (2012). SPOT5 imagery for soil salinity assessment in Iraq. Earth Resources and Environmental Remote Sensing/GIS Applications III, 8538, 85380V. doi:10.1117/12.974498.

[32] Howari, F. M. (2003). The use of remote sensing data to extract information from agricultural land with emphasis on soil salinity. Australian Journal of Soil Research, 41(7), 1243–1253. doi:10.1071/SR03033.

[33] Schneier-Madanes, G., & Courel, M.-F. (2010). Water and Sustainability in Arid Regions. Springer, Dordrecht, Netherlands. doi:10.1007/978-90-481-2776-4.

[34] Menenti, M., Lorkeers, A., & Vissers, M. (1986). An application of thematic mapper data in Tunisia. Estimation of daily amplitude in near-surface soil temperature and discrimination of hypersaline soils. Technical Bulletins, Institute for Land and Water Management Research, (54), 35–42.

[35] Madani, A. A. (2005). Soil salinity detection and monitoring using Landsat data: A case study from Siwa Oasis, Egypt. GIScience and Remote Sensing, 42(2), 171–181. doi:10.2747/1548-1603.42.2.171.

[36] Zhang, J., Liu, T., Feng, W., Han, L., Gao, R., Wang, F., Ma, S., Han, D., Zhang, Z., Yan, S., Yang, J., Wang, J., & Wang, M. (2025). Integrating Multi-Temporal Sentinel-1/2 Vegetation Signatures with Machine Learning for Enhanced Soil Salinity Mapping Accuracy in Coastal Irrigation Zones: A Case Study of the Yellow River Delta. Agronomy, 15(10), 2292. doi:10.3390/agronomy15102292.

[37] Soumaia, M. 'nassri, Asma, E. A., Basma, L., Asma, L., Balkis, C., Faiza, A. K., & Rajouene, M. (2025). Soil moisture and salinity disaggregation by integrating remote sensing data with the OPTRAM model. Environmental Earth Sciences, 84(16), 465. doi:10.1007/s12665-025-12453-4.

[38] Chen, Y., Qiu, Y., Zhang, Z., Zhang, J., Chen, C., Han, J., & Liu, D. (2020). Estimating salt content of vegetated soil at different depths with Sentinel-2 data. PeerJ, 8, 10585. doi:10.7717/peerj.10585.

[39] Duan, C., Zhang, Y., Hu, C., Chen, H., & Liu, P. (2025). Soil salinity inversion by combining multi-temporal Sentinel-2 images near the sampling period in coastal salinized farmland. Frontiers in Environmental Science, 13. doi:10.3389/fenvs.2025.1533419.

[40] Davis, E. (2018). Comparison of Sentinel-2 and Landsat 8 OLI in the Mapping of Soil Salinity in Hyde County, North Carolina. Master Thesis, University of South Carolina, Columbia, United States.

[41] Elshewy, M. A., Mohamed, M. H. A., & Refaat, M. (2024). Developing a Soil Salinity Model from Landsat 8 Satellite Bands Based on Advanced Machine Learning Algorithms. Journal of the Indian Society of Remote Sensing, 52(3), 617–632. doi:10.1007/s12524-024-01841-1.

[42] Wang, J., Peng, J., Li, H., Yin, C., Liu, W., Wang, T., & Zhang, H. (2021). Soil salinity mapping using machine learning algorithms with the sentinel-2 MSI in arid areas, China. Remote Sensing, 13(2), 1–14. doi:10.3390/rs13020305.

[43] Malenovský, Z., Rott, H., Cihlar, J., Schaepman, M. E., García-Santos, G., Fernandes, R., & Berger, M. (2012). Sentinels for science: Potential of Sentinel-1, -2, and -3 missions for scientific observations of ocean, cryosphere, and land. Remote Sensing of Environment, 120, 91–101. doi:10.1016/j.rse.2011.09.026.

[44] Taghadosi, M. M., Hasanlou, M., & Eftekhari, K. (2019). Retrieval of soil salinity from Sentinel-2 multispectral imagery. European Journal of Remote Sensing, 52(1), 138–154. doi:10.1080/22797254.2019.1571870.

[45] Wang, J., Ding, J., Yu, D., Ma, X., Zhang, Z., Ge, X., Teng, D., Li, X., Liang, J., Lizaga, I., Chen, X., Yuan, L., & Guo, Y. (2019). Capability of Sentinel-2 MSI data for monitoring and mapping of soil salinity in dry and wet seasons in the Ebinur Lake region, Xinjiang, China. Geoderma, 353, 172–187. doi:10.1016/j.geoderma.2019.06.040.

[46] Tahmoures, M., Honarbakhsh, A., Afzali, S. F., Nourzadeh Hadad, M., & Ostovari, Y. (2024). Quantifying salinity in calcareous soils through advanced spectroscopic models: A comparative study of random forests and regression techniques across diverse land use systems. Plos One, 19(8), e0307853. doi:10.1371/journal.pone.0307853.

[47] Gad, M. M. E. S., Mohamed, M. H. A., & Mohamed, M. R. (2022). Soil salinity mapping using remote sensing and GIS. Geomatica, 75(4), 295–309. doi:10.1139/geomat-2021-0015.

[48] De Keukelaere, L., Sterckx, S., Adriaensen, S., Knaeps, E., Reusen, I., Giardino, C., Bresciani, M., Hunter, P., Neil, C., Van der Zande, D., & Vaiciute, D. (2018). Atmospheric correction of Landsat-8/OLI and Sentinel-2/MSI data using iCOR algorithm: validation for coastal and inland waters. European Journal of Remote Sensing, 51(1), 525–542. doi:10.1080/22797254.2018.1457937.

[49] Douaoui, A. E. K., Nicolas, H., & Walter, C. (2006). Detecting salinity hazards within a semiarid context by means of combining soil and remote-sensing data. Geoderma, 134(1–2), 217–230. doi:10.1016/j.geoderma.2005.10.009.

[50] Khan, N. M., Rastoskuev, V. V., Shalina, E. V., & Sato, Y. (2001). Mapping salt-affected soils using remote sensing indicators-a simple approach with the use of GIS IDRISI, 22nd Asian Conference on Remote Sensing, 5-9 November, 2001, Singapore.

[51] Bannari, A., Guedon, A. M., El-Harti, A., Cherkaoui, F. Z., & El-Ghmari, A. (2008). Characterization of slightly and moderately saline and sodic soils in irrigated agricultural land using simulated data of advanced land imaging (EO-1) sensor. Communications in Soil Science and Plant Analysis, 39(19–20), 2795–2811. doi:10.1080/00103620802432717.

[52] Major, D. J., Baret, F., & Guyot, G. (1990). A ratio vegetation index adjusted for soil brightness. International Journal of Remote Sensing, 11(5), 727–740. doi:10.1080/01431169008955053.

[53] Abbas, A., & Khan, S. (2007). Using remote sensing techniques for appraisal of irrigated soil salinity. International Congress on Modelling and Simulation (MODSIM), 10-13 December, 2007, Christchurch New Zealand.

[54] Khan, N. M., Rastoskuev, V. V., Sato, Y., & Shiozawa, S. (2005). Assessment of hydrosaline land degradation by using a simple approach of remote sensing indicators. Agricultural Water Management, 77(1–3), 96–109. doi:10.1016/j.agwat.2004.09.038.

[55] Xu, C., Zeng, W., Huang, J., Wu, J., & Van Leeuwen, W. J. D. (2016). Prediction of soil moisture content and soil salt concentration from hyperspectral laboratory and field data. Remote Sensing, 8(1), 42. doi:10.3390/rs8010042.

[56] Yauri, R., Cuyubamba, L., & Nuñez, S. (2025). Crop Monitoring System Using IoT, Solar Energy and Decision Tree Algorithm. Emerging Science Journal, 9(2), 603–614. doi:10.28991/ESJ-2025-09-02-06.

[57] Abuelgasim, A., & Ammad, R. (2019). Mapping soil salinity in arid and semi-arid regions using Landsat 8 OLI satellite data. Remote Sensing Applications: Society and Environment, 13, 415–425. doi:10.1016/j.rsase.2018.12.010.

[58] Gerardo, R., & de Lima, I. P. (2022). Sentinel-2 Satellite Imagery-Based Assessment of Soil Salinity in Irrigated Rice Fields in Portugal. Agriculture (Switzerland), 12(9), 1490. doi:10.3390/agriculture12091490.

[59] Abd El-Hamid, H. T., & Hong, G. (2020). Hyperspectral remote sensing for extraction of soil salinization in the northern region of Ningxia. Modeling Earth Systems and Environment, 6(4), 2487–2493. doi:10.1007/s40808-020-00829-3.

[60] Ramos, T. B., Castanheira, N., Oliveira, A. R., Paz, A. M., Darouich, H., Simionesei, L., Farzamian, M., & Gonçalves, M. C. (2020). Soil salinity assessment using vegetation indices derived from Sentinel-2 multispectral data. application to Lezíria Grande, Portugal. Agricultural Water Management, 241, 106387. doi:10.1016/j.agwat.2020.106387.

[61] Kaplan, F., Bilgili, A. V., & Kılıç, M. (2026). Monitoring Soil Salinity in the Harran Plain: A Comparative Analysis of Machine Learning Algorithms Using Two Different Scenarios with Sentinel-2 Data. Eurasian Soil Science, 59(4), 65. doi:10.1134/S1064229325604706.

[62] Shi, S., Wang, Y., Wang, J., Yang, J., Bai, Z., & Peng, J. (2026). Soil Salinity Assessment and Cross-Regional Validation Based on Multiple Feature Optimization Methods and SHAP. Remote Sensing, 18(6), 955. doi:10.3390/rs18060955.

[63] Du, R., Chen, J., Zhang, Z., Chen, Y., He, Y., & Yin, H. (2022). Simultaneous estimation of surface soil moisture and salinity during irrigation with the moisture-salinity-dependent spectral response model. Agricultural Water Management, 265, 107538. doi:10.1016/j.agwat.2022.107538.

[64] Gorji, T., Yildirim, A., Hamzehpour, N., Tanik, A., & Sertel, E. (2020). Soil salinity analysis of Urmia Lake Basin using Landsat-8 OLI and Sentinel-2A based spectral indices and electrical conductivity measurements. Ecological Indicators, 112, 106173. doi:10.1016/j.ecolind.2020.106173.

[65] Elhag, M. (2016). Evaluation of different soil salinity mapping using remote sensing techniques in arid ecosystems, Saudi Arabia. Journal of Sensors, 2016(1), 7596175. doi:10.1155/2016/7596175.

[66] AL-Khakani, E. T., Al-Janabi, W. F., Sa'ad, R. Y., & Al-Kazaali, H. M. (2018). Using Landsat 8 OLI data to predict and mapping soil salinity for part of An-Najaf governorate. Ecology, Environment and Conservation, 24(2), 572-8.

[67] Günal, E., Wang, X., Kılıc, O. M., Budak, M., Al Obaid, S., Ansari, M. J., & Brestic, M. (2021). Potential of Landsat 8 OLI for mapping and monitoring of soil salinity in an arid region: A case study in Dushak, Turkmenistan. Plos one, 16(11), e0259695. doi:10.1371/journal.pone.0259695.

[68] Salem, O. H., & Jia, Z. (2024). Evaluation of Different Soil Salinity Indices Using Remote Sensing Techniques in Siwa Oasis, Egypt. Agronomy, 14(4), 723. doi:10.3390/agronomy14040723.

[69] Wang, F., Shi, Z., Biswas, A., Yang, S., & Ding, J. (2020). Multi-algorithm comparison for predicting soil salinity. Geoderma, 365, 114211. doi:10.1016/j.geoderma.2020.114211.

[70] Habibi, V., Ahmadi, H., Jafari, M., & Moeini, A. (2021). Mapping soil salinity using a combined spectral and topographical indices with artificial neural network. Plos One, 16(5), e0228494. doi:10.1371/journal.pone.0228494.